

Asymmetric charge trapping and emission kinetics in SiO_2/HfO_2 for accurate transistor reliability simulation

Guang-Hua Xu(徐光华), Shiyou Chen(陈时友), Yue-Yang Liu(刘岳阳)

Citation: Chin. Phys. B. 35, 097201 (2026). DOI: 10.1088/1674-1056/ae7db4 |
CSTR: 32038.14.CPB.ae7db4
http://cpb.iphy.ac.cn; http://iopscience.iop.org/cpb

What follows is a list of articles you may be interested in

Ultrafast reconfigurable direct charge trapping devices based on few-layer MoS_2

Hui Gao(高辉), Xuanye Liu(刘轩冶), Peng Song(宋鹏), Chijun Wei(尉驰俊), Nuertai Jiazila(努尔泰·加孜拉), Jiequn Sun(孙杰群), Kang Wu(吴康), Hui Guo(郭辉), Haitao Yang(杨海涛), Lihong Bao(鲍丽宏), Hong-Jun Gao(高鸿钧)
Chin. Phys. B. 33, 127201 (2024). DOI: 10.1088/1674-1056/ad8ecd

Quantitative measurement of the charge carrier concentration using dielectric force microscopy

Junqi Lai(赖君奇), Bowen Chen(陈博文), Zhiwei Xing(邢志伟), Xuefei Li(李雪飞), Shulong Lu(陆书龙), Qi Chen(陈琪), Liwei Chen(陈立桅)
Chin. Phys. B. 32, 037202 (2023). DOI: 10.1088/1674-1056/aca7e6

Evaluation of stress voltage on off-state time-dependent breakdown for GaN MIS-HEMT with SiN_x gate dielectric

Tao-Tao Que(阙陶陶), Ya-Wen Zhao(赵亚文), Qiu-Ling Qiu(丘秋凌), Liu-An Li(李柳暗), Liang He(何亮), Jin-Wei Zhang(张津玮), Chen-Liang Feng(冯辰亮), Zhen-Xing Liu(刘振兴), Qian-Shu Wu(吴千树), Jia Chen(陈佳), Cheng-Lang Li(黎城朗), Qi Zhang(张琦), Yun-Liang Rao(饶运良), Zhi-Yuan He(贺致远), Yang Liu(刘扬)
Chin. Phys. B. 29, 107201 (2020). DOI: 10.1088/1674-1056/abaed8

Experimental evaluation of interface states during time-dependent dielectric breakdown of GaN-based MIS-HEMTs with LPCVD-SiN_x gate dielectric

Ya-Wen Zhao(赵亚文), Liu-An Li(李柳暗), Tao-Tao Que(阙陶陶), Qiu-Ling Qiu(丘秋凌), Liang He(何亮), Zhen-Xing Liu(刘振兴), Jin-Wei Zhang(张津玮), Qian-Shu Wu(吴千树), Jia Chen(陈佳), Zhi-Sheng Wu(吴志盛), Yang Liu(刘扬)
Chin. Phys. B. 29, 067203 (2020). DOI: 10.1088/1674-1056/ab8895

Effect of transient space-charge perturbation on carrier transport in high-resistance CdZnTe semiconductor

Yu Guo(郭玉), Gang-Qiang Zha(查钢强), Ying-Rui Li(李颖锐), Ting-Ting Tan(谭婷婷), Hao Zhu(朱昊), Sen Wu(吴森)
Chin. Phys. B. 28, 117201 (2019). DOI: 10.1088/1674-1056/ab43bb

---

RAPID COMMUNICATION

Asymmetric charge trapping and emission kinetics in SiO_2/HfO_2 for accurate transistor reliability simulation

Guang-Hua Xu(徐光华)[1], Shiyou Chen(陈时友)[1,†], and Yue-Yang Liu(刘岳阳)[2,‡]

[1] *College of Integrated Circuits and Micro-Nano Electronics and Key Laboratory of Computational Physical Sciences (MOE), Fudan University, Shanghai* 200433, *China*

[2] *State Key Laboratory of Semiconductor Physics and Chip Technologies, Institute of Semiconductors, Chinese Academy of Sciences, Beijing* 100083, *China*

(Received 16 April 2026; revised manuscript received 10 June 2026; accepted manuscript online 16 June 2026)

Charge trapping in gate dielectrics governs reliability degradation in advanced transistors, and an essential mission is calculating the trapping rates of different defects accurately. Here, by high-throughput *ab initio* calculations, we demonstrate a significant asymmetric relaxation behavior of oxide defects during charge trapping and emission, and thus the predominantly assumed symmetric relaxation is invalid. Multiscale atomic-to-device simulations further reveal that the conventional symmetric approximation introduces orders-of-magnitude errors in charge transfer rates and qualitatively mischaracterizes the defect-resolved degradation. Therefore, we provide asymmetric relaxation data and corresponding modified charge trapping model for accurate reliability simulation of advanced transistors.

Keywords: charge trapping, high-*k*, gate dielectrics, reliability degradation, bias-temperature instability, *ab initio* calculations, multiscale simulation

PACS: 72.20.Jv, 77.55.df, 71.55.–i, 73.40.Qv

DOI: 10.1088/1674-1056/ae7db4 **CSTR:** 32038.14.CPB.ae7db4

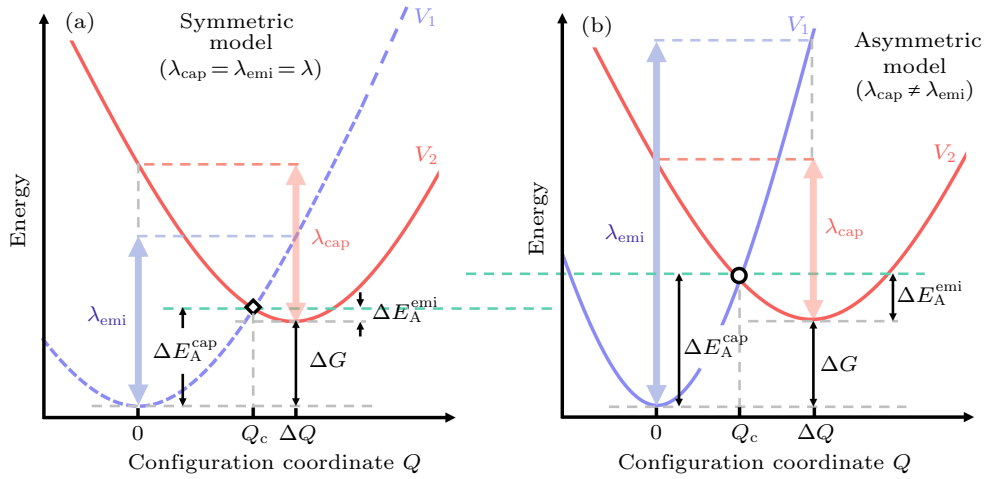
Charge trapping and emission are fundamental quantum-mechanical processes in semiconductor devices. On the one hand, charge trapping can be exploited as an operating mechanism in charge-trapping memories and reconfigurable devices.[1,2] On the other hand, charge trapping at defects in gate dielectrics is the microscopic origin of reliability degradation in metal–oxide–semiconductor field-effect transistors (MOSFETs), such as bias temperature instability (BTI),[3–6] random telegraph noise (RTN),[7–9] and dielectric breakdown (DB).[10–13] Therefore, charge trapping and emission kinetics must be accurately understood and controlled in different device contexts. Charge transfer theories, notably non-radiative multi-phonon (NMP) theory and Marcus theory, provide a robust physical framework for describing these processes.[14–17] Central to these theories is the configuration coordinate diagram (CCD),[18] in which activation barriers are determined by the crossing point of the initial and final state potential energy surfaces (PESs) relative to their respective minima. As illustrated in Fig. 1(a), the two PESs in the configuration-coordinate diagram have their own curvatures, which determine the relaxation energies for charge capture ($\lambda_{\rm cap}$) and emission ($\lambda_{\rm emi}$). Here, the curvature ratio is defined as $R = \sqrt{\lambda_{\rm emi}/\lambda_{\rm cap}}$, which characterizes the asymmetry between the capture and emission PESs through their relaxation energies. The conventional *symmetric approximation* assumes identical PES curvatures,[19] forcing $\lambda_{\rm emi} = \lambda_{\rm cap}$ and thus $R = 1$. Under this approximation, the capture and emission processes are described by symmetric parabolic PESs, so the crossing point and activation barriers can be obtained from the simplified symmetric expression in Fig. 1(c). This simplification has made the symmetric model the prevailing choice in reliability modeling.

In reality, however, structural relaxation paths for charge capture and emission often differ due to changes in local bonding environments,[20–22] corresponding to the asymmetric model shown in Fig. 1(b), where $\lambda_{\rm cap} \neq \lambda_{\rm emi}$. The barrier is then described in a more complex form as shown in Fig. 1(c). Despite this physical reality, the symmetric approximation continues to dominate reliability modeling, leaving the physically realistic asymmetric relaxation behavior largely overlooked. This raises a critical question: can the symmetric model faithfully reproduce the predictions of the rigorous asymmetric model? Answering this question requires first examining the relaxation energy data from atomistic calculations. Recent studies have indeed revealed relaxation energy asymmetry for SiO_2 defects.[21,22] Yet whether similar asymmetry exists for defects in HfO_2, the dominant high-*k* gate dielectric in scaled CMOS technologies,[23] remains largely unexplored. Furthermore, even where asymmetry has been identified, its quantitative impact on device-level reliability predictions has not been systematically evaluated.

†Corresponding author. E-mail: chensy@fudan.edu.cn

‡Corresponding author. E-mail: yueyangliu@semi.ac.cn

© 2026 Chinese Physical Society and IOP Publishing Ltd. All rights, including for text and data mining, AI training, and similar technologies, are reserved.



(c)

	Sym. model	Asym. model
Relaxation energy	$\lambda_{cap}=\lambda_{emi}=\lambda$	$\lambda_{cap}\neq\lambda_{emi}$
Curve ratio	$R=1$	$R\neq 1$
Crossing condition ($x=Q_c/\Delta Q$)	$2\lambda x-(\Delta G+\lambda)=0$	$(\lambda_{emi}-\lambda_{cap})x^2+2\lambda_{cap}x-(\Delta G+\lambda_{cap})=0$
Capture barrier (ΔE_A^{cap})	$\frac{(\lambda+\Delta G)^2}{4\lambda}$	$\frac{\lambda_{emi}}{(R^2-1)^2}\left(1-R\sqrt{\frac{\lambda_{emi}+(R^2-1)\Delta G}{\lambda_{emi}}}\right)^2$
Emission barrier (ΔE_A^{emi})	$\frac{(\lambda-\Delta G)^2}{4\lambda}$	$\frac{\lambda_{cap}}{(R^2-1)^2}\left(R^2-R\sqrt{\frac{\lambda_{emi}+(R^2-1)\Delta G}{\lambda_{emi}}}\right)^2$

Fig. 1. Schematic representation of configuration coordinate diagrams (CCDs) based on (a) the symmetric relaxation energy model and (b) the asymmetric model. (c) Comparison of the activation energy barrier expressions for the symmetric and asymmetric models.

In this work, we address this question through a multiscale investigation combining high-throughput *ab initio* calculations, charge transfer theory, and compact physics simulations. We first quantify the relaxation energy asymmetry for typical defects in SiO_2 and HfO_2, filling a notable data gap for advanced gate stacks. Based on the *ab initio* defect fingerprints, we then calculate charge transfer rates using Marcus theory and assess the model influence on threshold voltage shifts using the multiscale *ab initio* reliability simulator (MARS).[24] The multiscale results demonstrate significant discrepancies between the symmetric and asymmetric models, underscoring the necessity of incorporating asymmetric relaxation kinetics for reliability modeling and optimization of advanced MOSFETs.

The defect parameters were obtained via density functional theory (DFT) calculations using the PWmat software package[25] with a cutoff energy of 50 Ry. Amorphous SiO_2 and HfO_2 supercells, both containing 324 atoms, were used to model the dielectrics (see Fig. S1). The amorphous structures were generated by the bond switching Monte Carlo method.[26,27] Due to the large size of these supercells, the Brillouin zone was sampled at the single Gamma point. Structural optimizations were performed using the PBE functional[28] until the atomic forces converged to 0.01 eV/Å, and static calculations were carried out using the HSE hybrid functional[29] to ensure band gaps consistent with experimental values and gain suitable band alignment.[30] The investigated defects include oxygen vacancies (V_O), hydrogen bridges (HB), and hydroxyl groups (OH) in SiO_2, as well as V_O, hydrogen-substituted oxygen complex (V_O+H_i), and OH in HfO_2. Since all atomistic sites in amorphous structures are non-equivalent, we systematically sampled at least 30 different sites for each defect type to ensure statistical significance.

Figure 2 shows the statistical distributions of the calculated relaxation energies for hole capture (λ_{cap}, red) and emission (λ_{emi}, blue) for the six defect types. The results demonstrate that asymmetric relaxation energies are a general phenomenon rather than an exception. Specifically, SiO_2-V_O, SiO_2-OH, HfO_2-OH, and HfO_2-V_O+H_i exhibit significant asymmetry, characterized by a clear separation between the peak positions of the λ_{cap} and λ_{emi} distributions, as shown in Figs. 2(a)–2(d). In contrast, the distributions for SiO_2-HB and HfO_2-V_O show overlapping distributions, indicating near-symmetric relaxation energy, as shown in Figs. 2(e) and 2(f).

To investigate the kinetic impact of relaxation energy asymmetry, we first performed DFT calculations for the defect fingerprints, and then calculated the charge transfer rates using Marcus theory with the symmetric and asymmetric models (detailed formulas are given in the supplementary information S3). It should be noted that the defect parameters in

amorphous dielectrics are not single values but distributions. Each point in the parameter distribution corresponds to a specific CCD, activation barrier, and charge-transfer rate. Therefore, using the full distributions would lead to a set of CCDs and rate curves. To clearly illustrate the basic physical picture, Fig. 3 compares three representative defects: SiO_2-HB, HfO_2-V_O, and HfO_2-V_O+H_i, using CCDs constructed from the mean values of the parameter distributions summarized in Table S1. The electric field effect depends on the oxide electric field F_{ox} and the defect position x_t. In the rate calculation, this effect enters as the field-induced energy shift ($q \cdot F_{ox} \cdot x_t$), which shifts the defect level E_t and changes the crossing points of the potential-energy surfaces and thus the capture barriers. The resulting barrier differences are directly reflected in the predicted capture rate (k_{cap}) as a function of the field-induced energy shift, as shown in the bottom row.

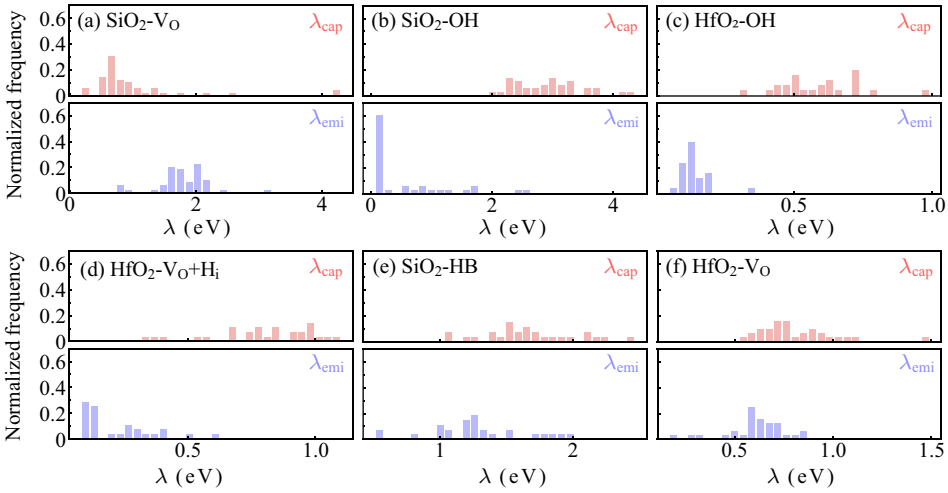


Fig. 2. Normalized frequency distributions of the relaxation energies for hole capture (λ_{cap}, red) and emission (λ_{emi}, blue) in SiO_2 and HfO_2, obtained from high-throughput *ab initio* calculations. The considered defects include (a) SiO_2-V_O, (b) SiO_2-OH, (c) HfO_2-OH, (d) HfO_2-V_O+H_i, (e) SiO_2-HB, and (f) HfO_2-V_O.

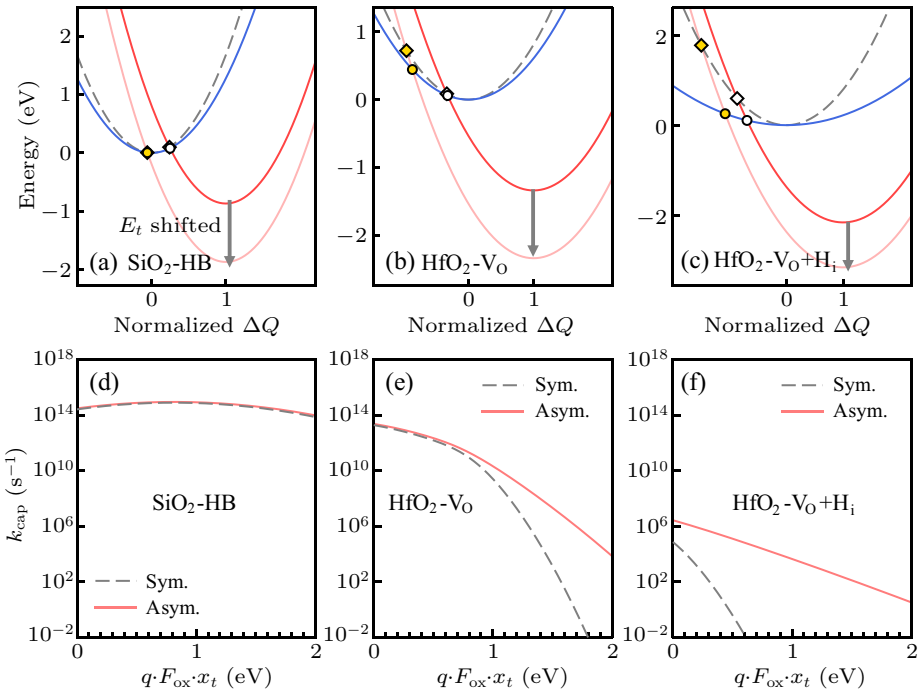


Fig. 3. Comparison of charge capture kinetics described by the symmetric and asymmetric models for three representative defects: SiO_2-HB, HfO_2-V_O, and HfO_2-V_O+H_i. (a)–(c) CCDs with grey dashed and blue solid lines representing initial-state parabolas for the symmetric and asymmetric models, respectively, and red final-state curves for unshifted E_t (opaque) and E_t shifted by 1 eV (semi-transparent). Circles and diamonds mark the crossing points. (d)–(f) Capture rates (k_{cap}) as a function of the field-induced energy shift ($q \cdot F_{ox} \cdot x_t$), where red solid lines represent asymmetric models and gray dashed lines represent symmetric approximation.

Strikingly, the symmetric approximation holds for SiO_2-HB but fails for HfO_2-V_O, even though both defects appear similarly near-symmetric in their relaxation energies. For SiO_2-HB, as shown in Fig. 3(a), the barrier difference between the symmetric and asymmetric models is only 0.02 eV at the unshifted case and shrinks to 0.005 eV after the field-

induced shift, yielding nearly identical rate curves as shown in Fig. 3(d). By contrast, HfO_2-V_O, despite having a similar curvature ratio ($R \sim 0.87$) to SiO_2-HB, exhibits a much stronger field response. As shown in Fig. 3(b), the barrier difference increases from 0.03 eV to 0.28 eV with E_t shifted, leading to a clear deviation in the high-field region. Consequently, the capture rates deviate in the high-field region, as shown in Fig. 3(e). Compared to SiO_2-HB and HfO_2-V_O, the model discrepancy is even more pronounced for HfO_2-V_O+H_i, where the barrier difference increases from 0.48 eV to 1.52 eV (Fig. 3(c)) and the predicted rates differ by several orders of magnitude (Fig. 3(f)).

This comparison reveals a critical finding that the validity of the symmetric approximation is governed not only by the curvature ratio R, but also by the absolute magnitudes of relaxation energies. Although SiO_2-HB and HfO_2-V_O share similar R values, the former has much larger relaxation energies ($\lambda_{cap} = 1.68$ eV, $\lambda_{emi} = 1.28$ eV) and lower defect level ($E_t = -0.81$ eV) than the latter ($\lambda_{cap} = 0.81$ eV, $\lambda_{emi} = 0.61$ eV, $E_t = 0.53$ eV). Larger relaxation energies and lower defect level of SiO_2-HB cause the parabolas to intersect at the flatter region, so the barrier difference between symmetric and asymmetric models remains small even after the shift in E_t, as shown in Fig. 3(a). When relaxation energies are smaller, however, the barrier becomes more sensitive to the energy shift and the discrepancy between the two models is amplified under high-field conditions, as shown in Fig. 3(b). Thus, the symmetric model can fail even for defects with apparently near-symmetric relaxation energies. Similar discrepancies between the two models are also observed for other defects, as shown in Fig. S2.

To evaluate the device-level impact of the model discrepancies, we further performed atomic-to-device NBTI simulations of a 28 nm commercial PMOS at 125 ° using the MARS simulator.[24] Whereas Fig. 3 uses mean defect parameters to illustrate the fundamental physical picture, Fig. 4 incorporates realistic defect distributions (Table S1) and compares the defect-resolved ΔV_{th} predicted by the two models. Hole trapping was simulated under stress at $V_g = -1.582$ V, followed by recovery at $V_g = -0.482$ V, as shown in Fig. 4(a). In the calculations of the threshold voltage shift (ΔV_{th}), the dielectric thickness was discretized into x_t grid positions, and the contribution from each grid point was weighted according to Eq. (7) in supplementary information S5, with the defect-specific parameter distributions included.

For SiO_2-HB (Fig. 4(b)), the symmetric model underestimates ΔV_{th}, even though the two models give nearly identical capture rates for the mean defect parameters (Fig. 3(d)). This originates from the distribution-integrated nature of device simulation, in which the mean parameters represent only one point in the x_t, E_t, λ_{cap}, λ_{emi} mesh array, whereas tail gridpoints in the full distribution can still contribute disproportionately. For these distribution-tail states, the asymmetric model predicts nearly complete occupation because emission becomes vanishingly small, while the symmetric model yields only moderate occupation. The resulting occupancy mismatch gives rise to an underestimated ΔV_{th} in the symmetric model.

HfO_2-V_O shows a similar trend to SiO_2-HB, with the symmetric model underestimating the degradation (Fig. 4(c)). The discrepancy becomes qualitative for HfO_2-V_O+H_i (Fig. 4(d)). The asymmetric model predicts degradation that accumulates over repeated stress-recovery cycles and remains only weakly recoverable, whereas the symmetric model predicts nearly constant trapped charge and hence a negligible ΔV_{th}. Thus, for this special defect type, the symmetric approximation does not merely underestimate the degradation. Instead, it misidentifies a partially permanent trapping behavior as essentially harmless. This failure arises from the extreme relaxation energy asymmetry of HfO_2-V_O+H_i, which causes the symmetric approximation to severely deviate from the rigorous asymmetric model in both capture and emission barriers, and consequently leads to a qualitatively incorrect device-level prediction. It should be noted that the corrections introduced by the asymmetric model are defect- and condition-dependent. Whether these corrections increase or decrease the capture/emission barriers, transition rates, and threshold-voltage shift should be analyzed for the specific defect parameters and bias conditions.

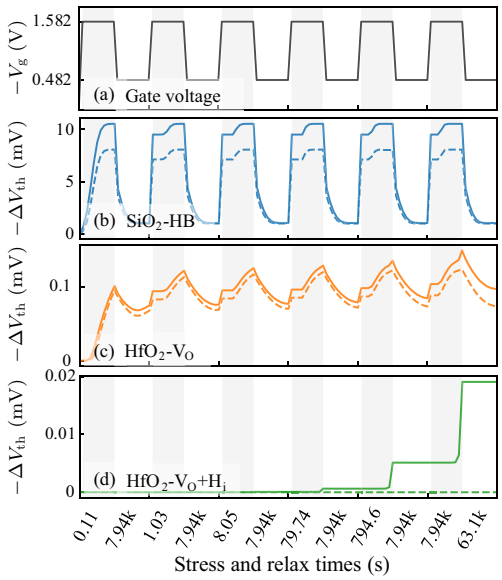


Fig. 4. (a) Gate voltage waveform used in the stress–recovery simulation. Stress and recovery were performed at $V_g = -1.582$ V and $V_g = -0.482$ V, respectively, at 125 °. Defect-resolved threshold voltage shifts (ΔV_{th}) during stress–recovery cycles for (b) SiO_2-HB, (c) HfO_2-V_O, and (d) HfO_2-V_O+H_i. Solid and dashed lines correspond to the asymmetric and symmetric models, respectively. Shaded and unshaded regions denote the stress and recovery phases, respectively, with the duration of each phase indicated at the bottom of the figure.

In conclusion, our multiscale analysis demonstrates that asymmetric relaxation energies are an intrinsic feature of de-

fects in both SiO_2 and HfO_2. The widely used symmetric approximation therefore neglects the asymmetric relaxation kinetics and can lead to orders-of-magnitude errors in rate predictions together with substantial misestimation of $\Delta V_{\rm th}$. For defects with highly asymmetric relaxation energies, the symmetric model can even misidentify partially permanent degradation as recoverable and thus produce qualitatively incorrect device-level behavior. Crucially, our results further show that apparent relaxation energy symmetry does not guarantee the validity of the symmetric approximation, which has not been recognized previously. This study underscores that the asymmetry of potential energy surfaces is a critical missing link in conventional reliability frameworks. Although our direct first-principles calculations and device-level simulations are performed for defects in SiO_2 and HfO_2, the physical origin of asymmetric relaxation is not limited to these two kinds of dielectrics. In amorphous oxides, the structural complexity and defect-specific relaxation paths after charge-state transitions generally make the relaxation energies for carrier capture and emission different. Therefore, asymmetric relaxation energies should be regarded as a broadly relevant feature of defects in other amorphous dielectrics, such as ZrO_2 and Al_2O_3. Ultimately, the paradigm shift from symmetric approximation to *ab initio*-informed asymmetric kinetics is essential for reliability modeling, understanding, and optimization of advanced semiconductor devices.

Acknowledgements

This work was supported by the National Key Research and Development Program of China (Grant No. 2024YFA1408200), the National Natural Science Foundation of China (Grant Nos. 12334005, 62174155, 12174060, 12188101, and 12404089), the CAS Project for Young Scientists in Basic Research (Grant No. YSBR-056), Science and Technology Commission of Shanghai Municipality (Grant No. 24JD1400600), and the MIND Project (Grant No. MINDKT202403).

References

[1] Gao H, Liu X, Song P, Wei C, Jiazila N, Sun J, Wu K, Guo H, Yang H, Bao L and Gao H J 2024 *Chin. Phys. B* **33** 127201
[2] You H W and Cho W J 2010 *Appl. Phys. Lett.* **96** 093506
[3] Cartier E, Linder B P, Narayanan V and Paruchuri V K 2006 *International Electron Devices Meeting*, December 11–13, 2006, San Francisco, CA, USA, p. 1
[4] Duhan P, Rao V R and Mohapatra N R 2017 *IEEE Trans. Electron Devices* **64** 4018
[5] Xu R R, Zhang Q Z, Zhou L D, Yang H, Gai T Y, Yin H X and Wang W W 2022 *Chin. Phys. B* **31** 017301
[6] Gong W T, Li Y, Sun Y B, Shi Y L and Li X J 2023 *Chin. Phys. B* **32** 128502
[7] Ralls K S, Skocpol W J, Jackel L D, Howard R E, Fetter L A, Epworth R W and Tennant D M 1984 *Phys. Rev. Lett.* **52** 228
[8] Kirton M J and Uren M J 1989 *Adv. Phys.* **38** 367
[9] Kaczer B, Toledano-Luque M, Goes W, Grasser T and Groeseneken G 2013 *Microelectron. Eng.* **109** 123
[10] Wu X, Migas D B, Li X, Bosman M, Raghavan N, Borisenko V E and Pey K L 2010 *Appl. Phys. Lett.* **96** 172901
[11] Nadimi E, Roll G, Kupke S, Ottking R, Planitz P, Radehaus C, Schreiber M, Agaiby R, Trentzsch M, Knebel S, Slesazeck S and Mikolajick T 2014 *IEEE Trans. Electron Devices* **61** 1278
[12] Xu H, Yang H, Luo W C, Xu Y F, Wang Y R, Tang B, Wang W W, Qi L W, Li J F, Yan J, Zhu H L, Zhao C, Chen D P and Ye T C 2016 *Chin. Phys. B* **25** 087305
[13] Liao Z Y, Fang P W, Lu X, Wang G and Pei Y L 2025 *Chin. Phys. B* **34** 067304
[14] Henry C Hand Lang D V 1977 *Phys. Rev. B* **15** 989
[15] Alkauskas A, Yan Q and Van De Walle C G 2014 *Phys. Rev. B* **90** 075202
[16] Rzepa G, Franco J, O'sullivan B, Subirats A, Simicic M, Hellings G, Weckx P, Jech M, Knobloch T, Waltl M, Roussel P J, Linten D, Kaczer B and Grasser T 2018 *Microelectron. Reliab.* **85** 49
[17] Liu Y Y, Zheng F, Jiang X, Luo J W, Li S S and Wang L W 2019 *Phys. Rev. Appl.* **11** 044058
[18] Stoneham A M 2001 *Theory of Defects in Solids: Electronic Structure of Defects in Insulators and Semiconductors*, online edn. (Oxford: Oxford Academic) pp. 477–552
[19] Grasser T 2012 *Microelectron. Reliab.* **52** 39
[20] Wimmer Y, El-Sayed A M, Gös W, Grasser T and Shluger A L 2016 *Proc. R. Soc. A* **472** 20160009
[21] Ma X, Liu Y Y, Zeng L, Chen J, Wang R, Wang L W, Wu Y and Jiang X 2021 *ACS Appl. Mater. Interfaces* **14** 2185
[22] Wilhelmer C, Waldhoer D, Jech M, El-Sayed A M B, Cvitkovich L, Waltl M and Grasser T 2022 *Microelectron. Reliab.* **139** 114801
[23] Mistry K, Chau R, Choi C H, *et al.* 2007 *IEEE International Electron Devices Meeting*, December 10–12, 2007, San Francisco, CA, USA, p. 247
[24] Liu Y Y, Xu G H, Xiong T, Li W F, Zhao Y, Liu T W, Wang Z, Wang R, Wang L W and Jiang X 2024 *IEEE International Electron Devices Meeting (IEDM)*, December 07–11, 2024, San Francisco, CA, USA, p. 1
[25] Jia W, Cao Z, Wang L, Fu J, Chi X, Gao W and Wang L W 2013 *Comput. Phys. Commun.* **184** 9
[26] Zheng F, Pham H H and Wang L W 2017 *Phys. Chem. Chem. Phys.* **19** 32617
[27] Zheng Z, Zheng F, Wu Y N, Chen S and Wang L W 2025 *Comput. Mater. Today* **6** 100031
[28] Perdew J P, Burke K and Ernzerhof M 1996 *Phys. Rev. Lett.* **77** 3865
[29] Heyd J, Scuseria G E and Ernzerhof M 2003 *J. Chem. Phys.* **118** 8207
[30] Li W F, Liu T W, Yang Z M, Wang L W and Liu Y Y 2025 *Chin. Phys. Lett.* **42** 017302